HOSTED BY

ELSEVIER

Available online at www.sciencedirect.com

ScienceDirect

Soils and Foundations 61 (2021) 1207–1222

www.elsevier.com/locate/sandf

Technical Paper

Post-liquefaction deformation and strength characteristics of sand in torsional shear tests

Muhammad Umar [a,e,*], Takashi Kiyota [b], Gabriele Chiaro [c], Antoine Duttine [d]

[a] Institute of Industrial Science, The University of Tokyo, Japan
[b] Institute of Industrial Science, The University of Tokyo, Japan
[c] Department of Civil and Natural Resources Engineering, University of Canterbury, New Zealand
[d] Director, Analytical Engineering Department, Integrated Geotechnology Institute Ltd, Japan
[e] National University of Computer and Emerging Sciences, Lahore, Pakistan

Received 25 September 2020; received in revised form 8 June 2021; accepted 10 June 2021
Available online 24 July 2021

Abstract

The estimation of strength deterioration with the increase in the undrained cyclic shear-induced strain in liquefiable soils is an important topic in geotechnical earthquake engineering that is still poorly understood and needs to be properly addressed. In this paper, in an attempt to provide new insights into this topic, the post-liquefaction undrained strength and deformation of Toyoura sand were investigated through a series of laboratory tests performed by using a large-strain torsional shear apparatus. In the tests, simple shear conditions were reproduced on a medium-size hollow cylindrical specimen to apply stress conditions that soil experiences in the field during earthquakes. Specimens prepared by the air-pluviation method were first liquefied by applying a constant amplitude undrained cyclic shearing to induce a target cyclic shear-induced damage strain (γ_{Δ}). The tests were terminated at different amplitudes of γ_{Δ} and subsequently loaded monotonically in undrained conditions to obtain stress-strain and excess pore water generation responses. The test results indicate that the post-liquefaction monotonic loading (ML) stress-strain behavior of sand can be divided into three regions, namely Region 1, 2 and 3. The sand behavior changes to strain-hardening from essentially zero strength and stiffness from Region 1 to 2. While Region 3 marks the beginning of strain-softening state in the sand. It is found that the strain localization is associated with the transition of sand behavior from strain-hardening to strain-softening state. It is proposed that the sand undrained strength in monotonic shearing is the true representation of specimen response until the state of uniform deformation is maintained, based on the sudden drop of the differential stress ($\sigma_d = \sigma'_v - \sigma'_h$). The test results also revealed that there is a progressive degradation in the shear strength with the increase in the amplitude of γ_{Δ}. A correlation depicting the degradation ratio (τ_d) with the increase in the γ_{Δ} is proposed. This correlation can be used to estimate the degree of degradation with the increase in the applied γ_{Δ}, and it is valid for different density states, confining stresses and cyclic stress ratios.

Keywords: Post-liquefaction; Multi-stage tests; Strength degradation; Torsional shear; Sand

1. Introduction

The effects of undrained cyclic loading (liquefaction) on undrained strength degradation have regained interest and become a subject of studies in recent years. During the 2011 Off the Pacific Coast of Tohoku Earthquake, a great number of earth structures, such as earth-fill dams and

Peer review under responsibility of The Japanese Geotechnical Society.

* Corresponding author.
E-mail addresses: umar@iis.u-tokyo.ac.jp (M. Umar), kiyota@iis.u-tokyo.ac.jp (T. Kiyota), gabriele.chiaro@canterbury.ac.nz (G. Chiaro), antoine@igi.co.jp (A. Duttine).

https://doi.org/10.1016/j.sandf.2021.06.009
0038-0806/

Nomenclature

CSR	Cyclic stress ratio
D_{50}	Particle mean diameter
D_i	Specimen's inner diameter
D_o	Specimens' outer dimeter
D_r	Relative density
e_{max}	Maximum void ratio
e_{min}	Minimum void ratio
EPWP	Excess pore water pressure
F_c	Fines content
G_1	Initial shear modulus
G_2	Intermediate shear modulus
G_3	Residual state shear modulus
G_s	Specific gravity
H	Specimen's height
p'	Effective mean principal stress
p'_0	Initial effective mean principal stress
r_d	EPWP degration ratio
t	Membrane thickness
γ_0	Threshold shear strain
γ_{DA}	Double amplitude shear strain
γ_L	Limiting shear strain to initiate strain localization
$\gamma_{L,DA}$	Double amplitude limiting shear strain
$\gamma_{L,SA}$	Single amplitude limiting shear strain
γ_{max}	Maximum shear strain
γ_{min}	Minimum shear strain
γ_{min}	Shear strain
γ_s	Softening strain
γ_Δ	Damage strain
$\gamma_{\Delta,max}$	Maximum damage strain
ΔU	EPWP ratio in undrained ML without γ_Δ
ΔU_{cyc}	EPWP ratio in undrained ML with $\gamma\Delta$
$\Delta\gamma_d$	Dilative strain
σ_d	Differential stress
σ'_h	Effective horizontal stress
σ'_v	Effective vertical stress
$\sigma_{z,m}/3$	Apparent vertical stress due to membranes
τ_{cyclic}	Cyclic shear stress
τ_d	Degradation strength ratio
τ_m	Apparent shear stress due to membranes
τ_p	Peak shear stress
$\tau_{p,max}$	Maximum peak shear stress
$\tau_{p,min}$	Minimum peak shear stress
τ_{PL}	Undrained limiting strength in the reference ML (with $\gamma_\Delta = 0$ after liquefaction)
$\tau_{PL\Delta}$	Undrained limiting strength in ML with γ_Δ

embankments suffered extensive damages, such as the disastrous slope failure of Fujinuma Dam in Fukushima Prefecture, Japan. The Fujinuma Dam failure caused uncontrolled release of reservoir flooding and destroyed the community immediately downstream. A comprehensive investigation by Tatsuoka et al. (2017) revealed that a likely scenario of Fujinuma Dam collapse is the degradation of undrained strength of the dam body formed by sandy soil due to a prolonged cyclic undrained loading during the earthquake. Based on this, Tatsuoka et al. (2017) and Duttine et al. (2018) proposed a new simplified seismic stability analysis (Newmark-D) taking into account the continuous degradation of undrained stress-strain properties to evaluate the seismic performance of earth-fill-dams.

Most of the last decade of laboratory-based research has mainly focused on the fundamental understanding of the mechanism of pore water pressure and undrained behavior leading to liquefaction during cyclic loading. However, comprehensive attempts to understand the post-liquefaction strength characteristics of sandy soils have been limited (e.g. Zhang and Wang, 2012; Lombardi et al., 2017). One of the reasons for this is technical difficulty in achieving large deformation (i.e. double amplitude shear strain $\gamma_{DA} > 20\%$), and another challenge is the large extent deformation in non-uniform specimens at large strain levels using conventional laboratory tests, such as simple shear and triaxial tests.

Vaid and Thomas (1995) investigated the undrained strength of liquefied specimens (herein referred to as post-liquefaction) through triaxial tests. The specimens were liquefied by a constant amplitude cyclic loading and subsequently loaded monotonically. They reported that the stress-strain plot showed continuous recovery in stiffness and strength and there was no tendency towards the residual state in sand (strain-softening response with the reduction in the stiffness and strength). Dash (2010) conducted similar triaxial tests on medium dense Toyoura sand and showed that the stiffness is comparable between the liquefied and non-liquefied specimens. Rouholamin et al. (2017) reported that the stiffness during undrained monotonic loading in liquefied dense specimens is higher as compared to loose specimens. Both the loose and the dense sands investigated by Rouholamin et al. (2017) showed continued dilation in a liquefied specimen during undrained monotonic loading and strain-softening was not observed.

To reproduce the soil seismic response in the laboratory, it is well accepted that simple shear tests accurately simulate the condition of field expected during earthquakes, and are more reliable than triaxial tests (Boulanger et al., 1993; among others). A torsional simple shear test on a hollow cylindrical specimen has an advantage over triaxial tests in reproducing more realistic in-situ stress conditions. Also, unlike the triaxial test, the torsional shear apparatus

can mimic the rotation of major principal stress direction during the loading process. Yasuda et al. (1995) and Shamoto et al. (1997) conducted torsional shear tests to investigate the post-liquefaction strength and deformation of Toyoura sand following the methodology of Vaid and Thomas (1995). Their findings were consistent with the Vaid and Thomas (1995) and they characterized the liquefied sand stress-strain response into two regions. The first region represents the sand deformation under the state of zero shear stress, while in the second region, the strength and stiffness of the specimen is recovered by mobilization of positive dilatancy (Fig. 1).

The phenomenon of unchanged stiffness and strength with strain in soils is opposite to the commonly assumed behavior, and straining is associated with a reduction in stiffness and shear strength. Yasuhara et al. (1997) conducted undrained triaxial tests by subjecting a sandy specimen to cyclic non-reversal loading. Non-reversal loading prevents the specimen from reaching the state of liquefaction and progressive deformation accumulates in the specimen with the cyclic loading (Hyodo et al., 1991; Chiaro et al., 2012). They reported that the specimen strength and stiffness deteriorated compared to undrained monotonic loading test by increasing the cyclic loading history. They proposed a correlation representing the sand deterioration in the post-cyclic undrained strength with the increase in the cyclic loading history. To the best of knowledge of the author, a general relationship between the post-liquefaction undrained strength degradation with the increase in cyclic loading induced-strain (herein referred to as damage strain) for sandy soils has not been determined, or even approximated. Presently an empirical approach based on case studies (Seed, 1987) has been widely used in practice to estimate the undrained strength of the liquefied soil.

The lack of understanding between the post-liquefaction undrained strength degradation with the increase in cyclic loading induced-strain for sandy soils can be attributed to the limitations in the existing available laboratory tools to fully simulate post-liquefaction undrained monotonic behavior of sands. For instance, a liquefied specimen subjected to undrained monotonic compressional loading in triaxial will generate negative excess pore water pressure by mobilization positive dilatancy. Consequently, the effective stress in the specimen will continue to increase before reaching a state of cavitation or boiling. The state of cavitation represents the specimen change in response from undrained to drained and consequently the tests results become unrepresentative (McManus and Davis, 1997). In the case of torsional shear tests, the majority of previous studies (e.g. Tatsuoka et al., 1982; Shamoto et al., 1997; Georgiannou et al., 2008) used a relatively smaller specimen (i.e., 100 mm in height and diameter/height ratio of 1) and sand behavior could have been affected by bedding error. Also, there was limited capacity to measure the torsional load and negative excess pore water pressure.

On the other hand, by using a novel torsional shear apparatus capable of achieving γ_{DA} exceeding 100%, Kiyota et al. (2008), Chiaro et al. (2012, 2013, 2021) and Umar et al. (2021) were able to investigate the large deformation behavior of liquefied sand during undrained cyclic loading in the case of both level and sloping ground conditions. In such tests, the strain localization (i.e., formation of shear band) took place at large strains levels (e.g. for medium dense sand it occurred at $\gamma_{DA} > 28\%$). However, the monotonic post-liquefaction strength characteristics of sand under torsional simple shear conditions were not scrutinized in such studies.

In this study, the post-liquefaction undrained strength of sand was investigated by using the large-strain torsional apparatus developed by Kiyota et al. (2008). Careful consideration was made to accurately determine the effects of specimen size and testing conditions to accurately simulate undrained response of sand. A series of tests were performed to investigate shear strength of liquefied loose and dense Toyoura sand specimens adopting the methodology proposed by Yasuda et al. (1995). The post-liquefaction monotonic behavior is compared with the non-liquefied (i.e. undrained monotonic) one and a systematic comparison is made in terms of the stress-strain, excess pore water generation, and differential stress relationships.

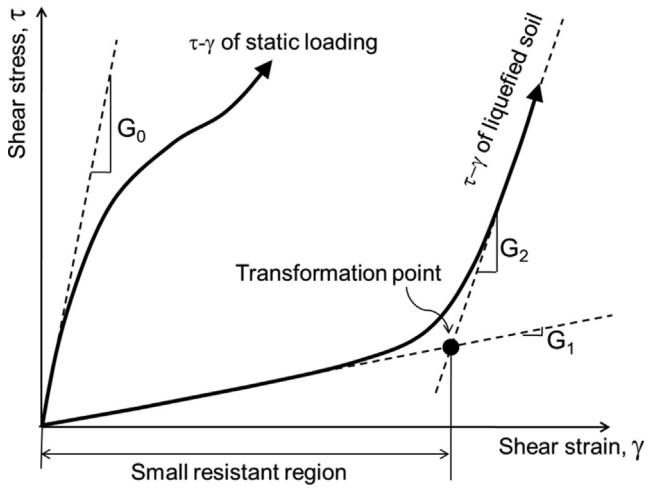

Fig. 1. General stress-strain model for liquefied soil (Vaid and Thomas, 1995; Yasuda et al., 1995; among others).

2. Apparatus, material, testing procedure and membrane correction

Fig. 2 shows the large-strain torsional shear apparatus used in this study. The full details of the apparatus and the stress computations have been comprehensively described by Chiaro et al. 2012, 2021. The experiments were performed on Toyoura sand ($G_s = 2.659$, $e_{max} = 0.951$, $e_{min} = 0.608$), which is a uniform quartz-rich sand with sub-angular particles with mean diameter (D_{50}) of 0.18 mm and negligible fines content ($F_c < 0.1\%$). The

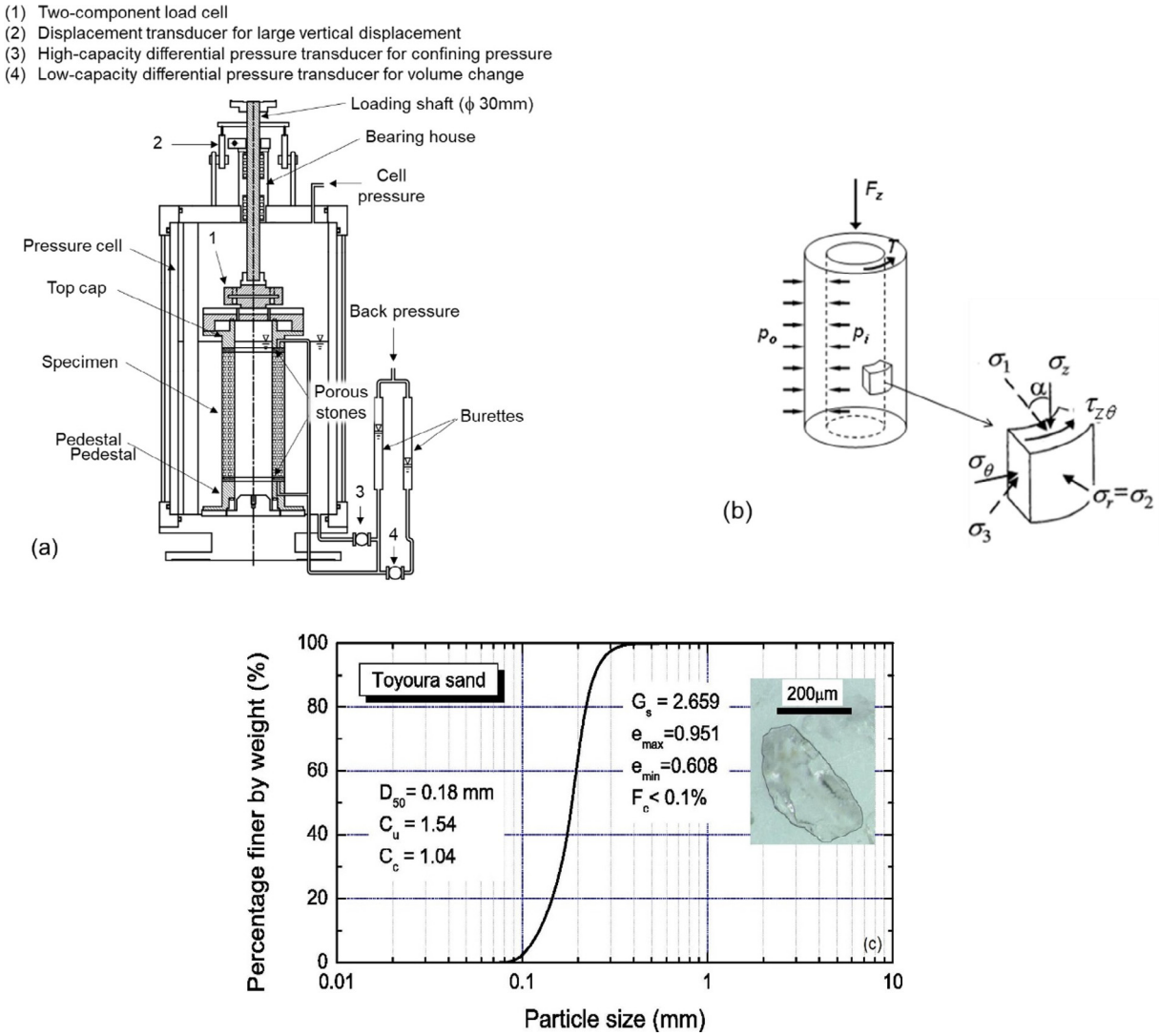

Fig. 2. (a) Torsional shear apparatus employed in this study (adopted from Kiyota et al., 2008); (b) External forces and stress components acting on a hollow cylindrical specimen (adopted from Chiaro et al., 2017); and (c) Particle size distribution of Toyoura sand investigated in this study.

particle size distribution of Toyoura sand and a photo of its typical grain are shown in Fig. 2c.

In this study, to perform as many tests as possible within a limited period of time, a smaller specimen (height $H = 200$ mm, outer diameter $D_o = 100$ mm, and inner diameter $D_i = 60$ mm) was adopted as compared to that used by Kiyota et al. (2008) ($H = 300$ mm, $D_o = 150$ mm, $D_i = 90$ mm). Umar et al. (2018) showed that the undrained monotonic and cyclic torsional shear deformation characteristics are essentially consistent among these two specimen sizes. The specimens were prepared by air pluviation method to form hollow cylindrical specimens. Air-dried sand was poured through a funnel at a constant pluviation height to achieve the formation of specimens with uniform relative density.

To investigate the influence of density state on the post-liquefaction strength degradation and deformation characteristics of Toyoura sand, specimens were prepared at a relative density (D_r) of 49 ± 3% (loose) and 70 ± 3% (dense). A high degree of saturation (i.e. Skempton's B-value > 0.95) was achieved by employing the double vacuum method (Ampadu, 1991). The specimens were kept under double vacuum for 1 h and subsequently, de-air water was circulated into the specimens.

The experimental procedure to study post-liquefaction characteristics in a two-stage sequence is adopted from Yasuda et al. (1995), and is schematically illustrated in Fig. 3. In the first stage, the specimens were isotropically consolidated by increasing the effective stress up to the desired level while keeping a back pressure of 200 kPa (state A). Afterward, undrained constant-amplitude cyclic torsional shear stress was applied at a shear strain rate of 0.5%/min from state A to B. The cyclic loading was terminated upon reaching the desired amplitude of damage strain (γ_Δ) that represents the amount of shear strain a sand specimen may experience after achieving the full liquefaction state ($p' = 0$). Such strain will induce a change of the specimen soil structure/fabric weakening the

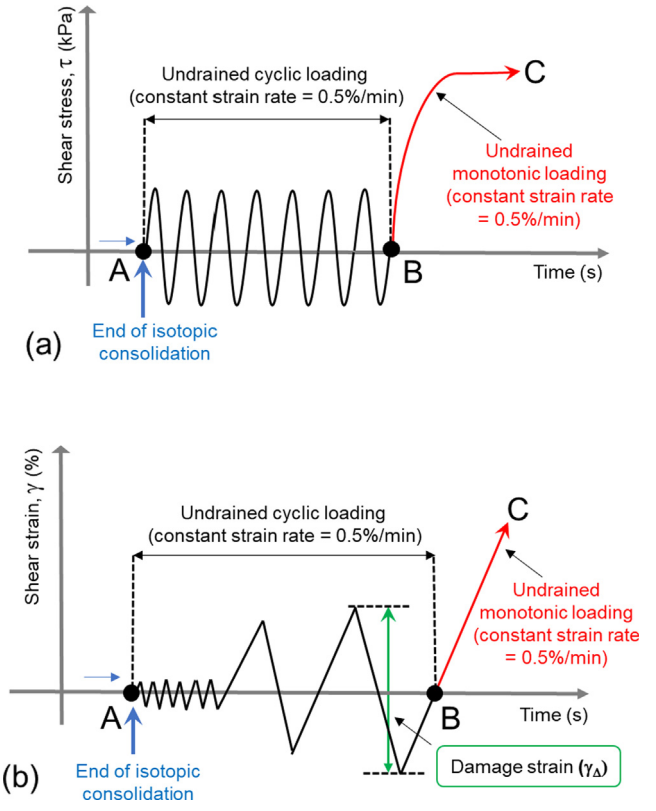

Fig. 3. Schematic illustration of the adopted test loading conditions: (a) shear stress vs time relationship; and (b) shear strain vs time relationship.

particle–particle contacts and affect the undrained shear strength of sand as compared to a reference condition where no shear strain takes place after liquefaction. This γ_Δ is defined by Eqn. (1) and illustrated in Fig. 3.

$$\gamma_\Delta = \gamma_{max} - \gamma_{min} \quad (1)$$

where γ_{max} and γ_{min} are the maximum shear strain in the clockwise and anti-clockwise loading directions, respectively.

In the second stage (from state B to C), undrained monotonic shear loading was applied (i.e., the drainage valve was kept closed) after the specimen achieved the desired γ_Δ. During the process of undrained loading, the vertical displacement of the top cap was mechanically prevented to simulate a quasi-simple shear condition (Kiyota et al., 2008). A summary of the tests performed is provided in Table 1.

2.1. Membrane force corrections

In torsional shear tests on hollow cylindrical soil specimens, the effect of membrane force on measured torsional shear stress cannot be neglected (Koseki et al., 2005). Specifically, to calculate the shear stress effectively applied on the soil specimen, the total stress measured by the load cell needs to be corrected for the apparent shear stress induced by the presence of the latex membranes. In a similar manner, the mean effective stress requires amendments due to membrane force effects as well (Chiaro et al., 2013).

Fig. 4 shows the comparison of the result from water specimens ($H = 300$ mm; $D_o = 150$ mm; $D_i = 90$ mm; membrane thickness $t = 0.2$ mm) tested by Chiaro et al. (2012) with that used in this study ($H = 200$ mm, $D_o = 100$ mm; $D_i = 60$ mm; $t = 0.2$ mm). The results are compared in terms of shear strain (γ) and apparent shear stress (τm). Fig. 4 shows that the size of the specimen has negligible effects on the membrane force. Therefore, the empirical hyperbolic correlation suggested by Chiaro et al. (2021) is still valid and was employed in this study to correct the applied shear stress. Alternatively, the effective mean principal stress was corrected for the membrane force effect by using the linear expression between the apparent vertical stress due to membranes ($\sigma_{z,m}/3$) and the γ as suggested by Chiaro et al. (2021).

3. Test results

3.1. Development of damage strain

Typical effective stress paths and stress-strain relationships are presented for typical loose and dense specimens in Figs. 5 and 6, respectively. The specimens were isotopically consolidated at the mean principal effective stress (p'_0) of 100 kPa and subjected to cyclic shear stress ratio ($CSR = \tau_{cyclic}/p'_0$, which is defined as the ratio between the cyclic shear stress, τ_{cyclic}, and the initial effective mean stress, p'_0) of 0.20. The cyclic loading was terminated after achieving γ_Δ of 13% and 12% in the loose and dense specimens, respectively.

Figs. 5a and 6a show that both the loose and dense specimens have contractive behavior (leading to a decrease in the p'_0 value) upon cyclic shearing. The p'_0 decreased with the increase in the number of shear loading cycles and ultimately the specimen achieved the zero effective stress state ($p'_0 = 0$), hereafter referred to as the full liquefaction state. Cyclic mobility was observed in the effective stress path where the effective stress recovered repeatedly after reaching $p'_0 = 0$. It was accompanied by a significant development of shear strain in the subsequent loading cycles in both the loose and dense specimens, as can be observed by the stress-strain relationship in Figs. 5b and 6b. This behavior is commonly observed in the laboratory and is known as typical result of a liquefaction test. Following the cyclic loading, in the post-liquefaction undrained monotonic shear loading stage, the stress path followed steadily the failure envelop (Figs. 5a and 6a), while the shear strain continued to increase gradually (Figs. 5b and 6b). The smooth stress-strain trends abruptly ended when strain localization took place, due to non-uniform deformation occurring in the specimens. Therefore, in this study, although reported for completeness, any data points after the strain localization state were not considered in the strength analyses reported hereafter.

Table 1
Summary of undrained torsional shear tests performed in this study.

Test No.	Relative Density, D_r (%)	Damage strain, γ△%	Effective mean effective stress, p'_0 (kPa)	Cyclic stress ratio, CSR = τ_{cyclic}/p'_0
1-1	49.0	0	100	ML(NL)*
1-2	47.9	1#	100	0.20
1-3	48.3	6	100	0.20
1-4	52.2	13	100	0.20
1-5	47.1	15	100	0.20
1-6	50.8	22	100	0.20
1-7	49.0	24	100	0.20
2-1	73.3	0	100	ML(NL)*
2-2	68.7	3#	100	0.20
2-3	72.1	8	100	0.20
2-4	67.9	12	100	0.20
2-5	70.1	19	100	0.30
3-1	48.0	0	150	ML(NL)*
3-2	49.0	6	150	0.20
3-3	50.0	0	200	ML(NL)*
3-4	47.2	0	400	ML(NL)*
4-1	47.9	6	100	0.12
4-2	48.3	6	100	0.17

* ML(NL): Monotonic undrained test without liquefaction (i.e. conducted just after consolidation).
# Reference monotonic post-liquefaction tests (i.e. monotonic loading applied immediately after full liquefaction state ($p' = 0$) with least damage shear already taking place).

3.2. Post-liquefaction monotonic stress-strain behavior

Fig. 7a and 7b show the stress-strain relationships for the loose and dense specimens during the second stage of loading (i.e., undrained monotonic). Each stress-strain curve represents a test with the cyclic loading history of γ_Δ and their details are provided in Table 1.

According to Fig. 7a and b, the loose and dense specimens deformed under essentially zero stiffness and shear strength up to a transformation point (hereby will be referred to as transformation point 1, TP1 (note that TP1 has been referred to as the threshold shear strain (γ_0) by Yasuda et al. (1995) and Zhang and Wang (2012) as illustrated in Fig. 1). The rate of the increment in the stiffness (represented by the slope of stress-strain curve) of the sand specimens progressively increased after the γ_0 and subsequently achieved a state of constant increment (i.e., the inclination of the stress-strain curve becomes linear). The mobilization of positive dilatancy induced by particle rearrangement is associated with the increase in stiffness and strength in a liquefied specimen. These characteristics are consistent with Vaid and Thomas (1995) and Yasuda et al. (1995) for liquefied specimens subjected to undrained monotonic loading. Zhang and Wang (2012) successfully simulated the post-liquefaction stress-strain as well the development of γ_0 by a simple constitutive model considering the dilatancy during undrained conditions.

The results reported in Fig. 7a and 7b show that the sand stiffness and strength reached a second transformation point (i.e., TP2), in correspondence of the change in the inclination of the stress-strain curve. The peak shear stress state deteriorated with the increase in the amplitude of γ_Δ as compared to that of the monotonic test (ML) without γ_Δ. This is expected as larger γ_Δ consumed more dilatancy, and less dilatancy mobilizes lower peak shears stress. Both the loose and dense specimens showed degradation in the peak shear stress. This kind of response is natural as straining causes a reduction in the stiffness and shear stress in soils (Yasuhara et al., 1992; Song et al., 2004).

Fig. 8a and b show the excess pore water pressure generation (EPWP = 1- (p'/p'_0)) ratio variation against shear strain for loose and dense specimens during undrained ML. Each EPWP curve displays a test with the cyclic loading history of γ_Δ. The results show that the recovery in the EPWP started after TP1. The EPWP for both the loose and dense specimens showed TP2, similar to the stress-strain responses (Fig. 7a and 7b). The values of the EPWP also showed deterioration with the increase in the amplitude of γ_Δ compared to the ML tests for the respective density state.

3.2.1. Effect of cyclic shear stress on the post-liquefaction deformation

It is well known that the resistance against EPWP reduces with the increase in the applied *CSR* at the same confining stress. Therefore, to identify the dependency of *CSR* on the post-liquefaction ML peak shear state and EPWP, three specimens were prepared at a D_r of approximately 48% and consolidated at $p'_0 = 100$ kPa. They were subsequently subjected to a *CSR* of 0.12, 0.17, and 0.20 to achieve $\gamma_\Delta$of 6%. The stress-strain relationships and EPWP paths during post-liquefaction undrained ML are shown in Fig. 9.

Despite the difference in the *CSR*, Fig. 9a shows that the TP1 appeared at the same amplitude of γ_0 for the three specimens. This is in agreement with the findings reported by Wang et al. (2016a) and (Hu et al., 2020) through

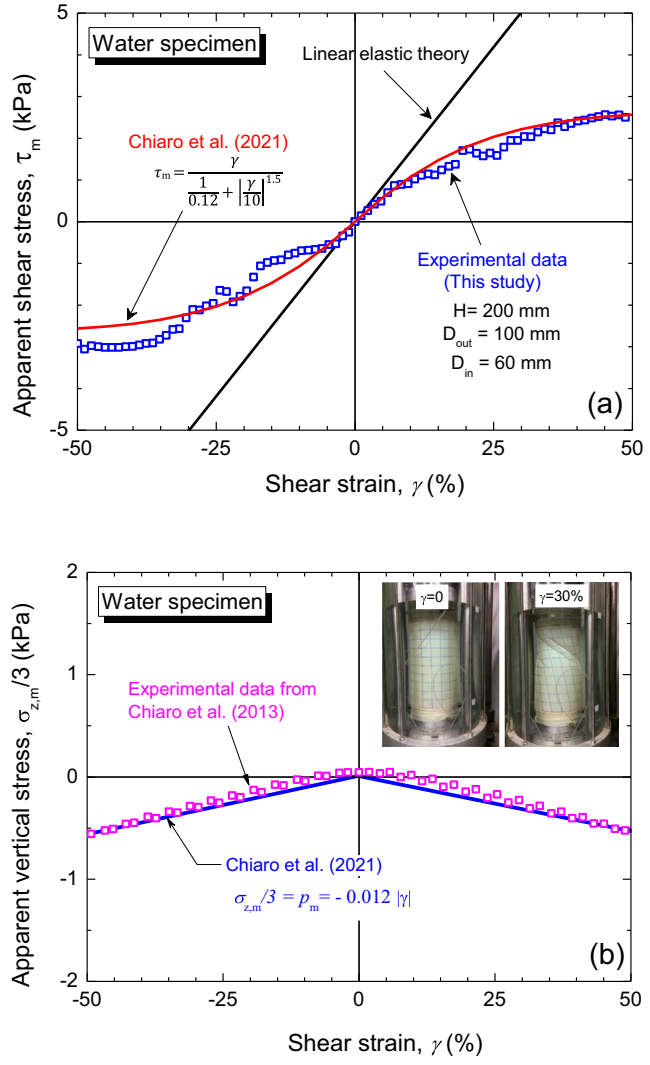

Fig. 4. Experimental evaluation of membrane forces and their corrections: (a) apparent shear stress-strain relationship; and (b) apparent vertical stress-strain relationship.

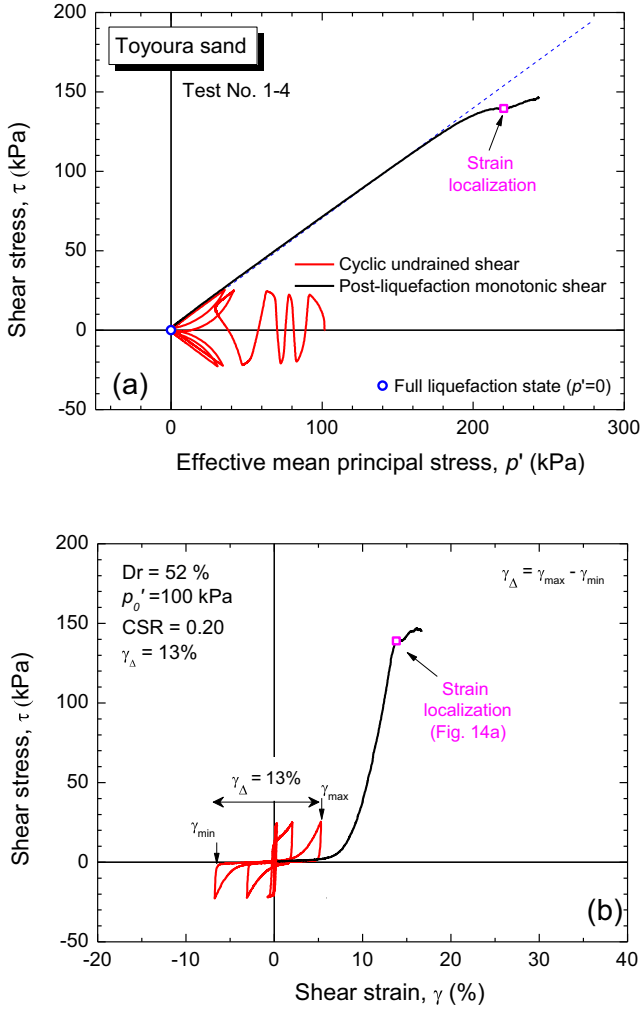

Fig. 5. Typical undrained torsional shear test results for loose Toyoura sand subjected to $\gamma_\Delta = 13\%$ ($D_r = 52\%$; $CSR = 0.20$): (a) Effective stress path; and (b) stress-strain relationship.

discrete element modeling tests. Also, the specimens achieved TP2 at the identical peak shear stress and strain. Following TP2, the three specimens continued to deform under the constant state of shear stress. The EPWP showed similar characteristics for the three specimens as can be seen in Fig. 9b. These results imply that post-liquefaction monotonic response mainly depends on the development of γ_Δ and is unaffected by the amplitude of cyclic shear stress. From a practical perspective, for the same level of γ_Δ, the stress amplitude variation during earthquakes has insignificant influence on strength deterioration.

3.2.2. Characterization of post-liquefaction stress-strain response

To investigate the post-liquefaction undrained ML deformation behavior in detail, the response of a dense specimen subjected to $\gamma_\Delta = 19\%$ is plotted individually in Fig. 10 in terms of stress-strain relationship and EPWP path.

The initial portion of the stress-strain plot in Fig. 10a has an initial slope defined by the initial shear modulus (G_1) at the beginning of the ML. After the TP1, the specimen transitioned into the intermediate state shear modulus (G_2) after exceeding the threshold strain γ_0 (Yasuda et al., 1995; Rouholamin et al., 2017). The EPWP showed similar characteristics, as can be seen in Fig. 10b: it decreased suddenly from the initial value of 100 kPa (full liquefaction state, $p' = 0$).

Fig. 10a indicates also the transition of G_2 into a residual state shear modulus (G_3) following TP2. The EPWP at TP2 exhibited similar characteristics (Fig. 10b). It is clear that the TP2 takes place at the same shear strain level on the stress-strain and EPWP plots. This indicates that the sand specimen has mobilized positive dilatancy and transitioned into a strain softening state. Note that the shear strain level at this state is referred to hereafter as softening strain (γ_s).

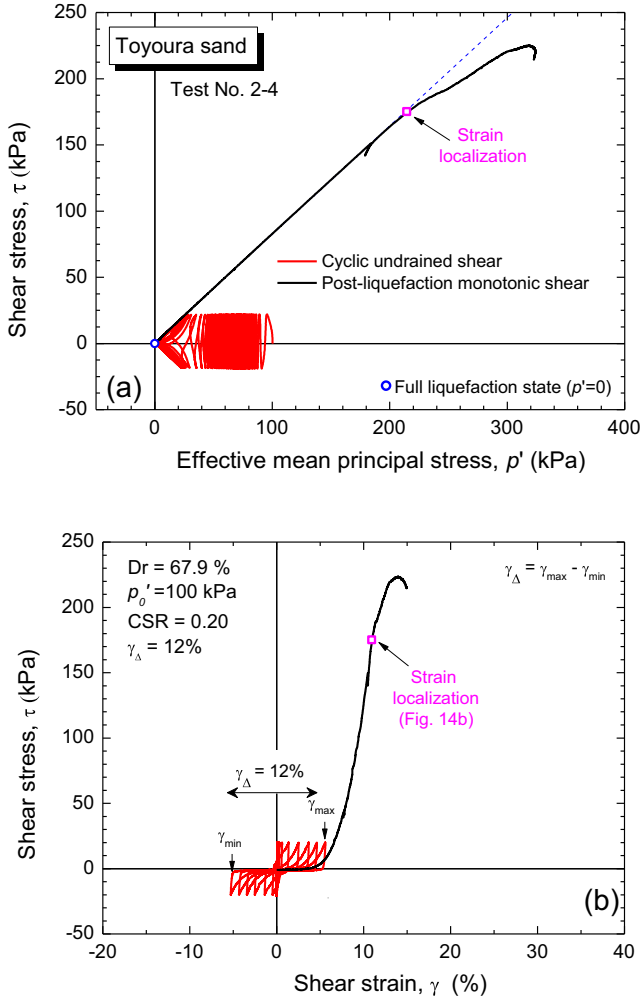

Fig. 6. Typical undrained torsional shear test results for dense Toyoura sand subjected to $\gamma_\Delta = 12\%$ ($D_r = 67.9\%$; $CSR = 0.20$): (a) Effective stress path; and (b) stress-strain relationship.

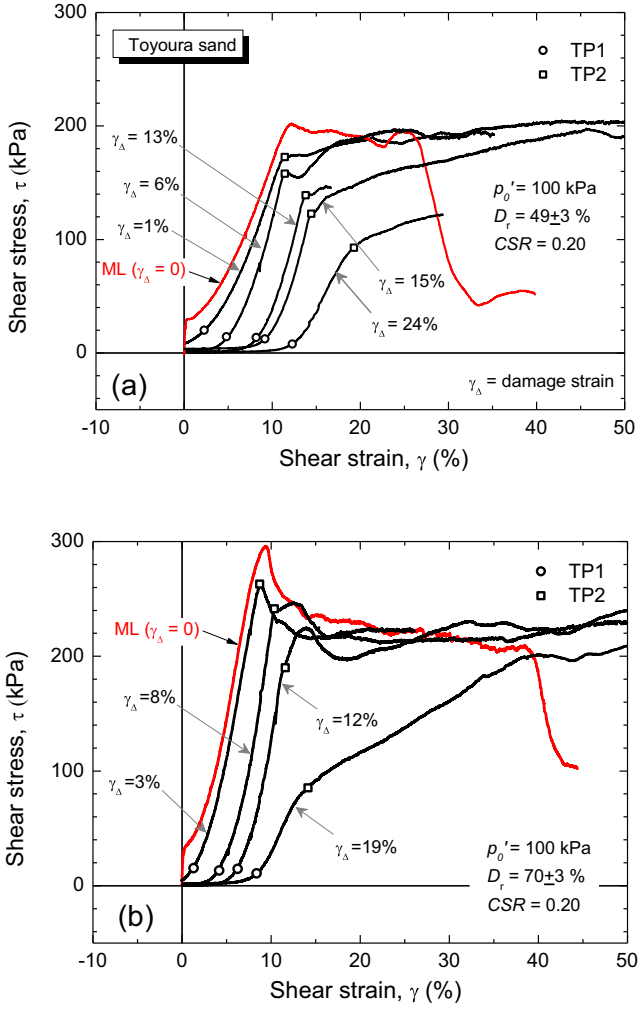

Fig. 7. Post-liquefaction stress-strain responses of (a) loose ($Dr = 49 \pm 3\%$) and (b) dense ($Dr = 70 \pm 3\%$) Toyoura sand in undrained torsional shear tests with various damage strain levels.

Based on the above, post-liquefaction undrained ML stress-strain behavior can be divided into three distinct regions: Regions 1, 2 and 3. *Region 1* spans from the state at which the specimen develops shear strain under zero effective stress and nearly-zero shear modulus G_1. *Region 2* begins with a transition into a G_2, with an accelerated recovery in strength over small strain increments - the linear segment of the stress-strain relationship represents a constant G_2. *Region 3* corresponds to the change in the stress-strain curve slope and transition of shear modulus, G_3 from G_2 at γ_s. The difference in the strain level between γ_s and γ_0 is defined here as the dilative strain ($\triangle\gamma_d$). The $\triangle\gamma_d$ is an indicator of how much shear strain a sand specimen develops from mobilization of the positive dilatancy to the residual state. The definition of γ_0, γ_s, and $\triangle\gamma_d$ is provided in Fig. 10.

Fig. 11 shows variations in γ_0 and $\triangle\gamma_d$ with increasing γ_Δ for loose and dense sand specimens. It can be seen that the value of γ_0 at TP1 increased with the amplitude of γ_Δ. The loose specimen required a larger γ_0 than the dense specimen to mobilize the positive dilatancy during ML. The value of γ_0 for the dense as well as loose specimens increased with the increase in the amplitude of γ_Δ due to strain-induced softening by cyclic loading. Also, the results indicate that the history of γ_Δ is delayed in the sand particle–particle interlocking, thus mobilizing positive dilatancy. This trend is similar to those reported by Zhang and Wang (2012) and Hu et al. (2020). On the other hand, the $\triangle\gamma_d$ response is opposite to that of γ_0 and essentially unaffected by the initial density. Yet, the value of $\triangle\gamma_d$ decreased with the increase in the amplitude of γ_Δ. This suggests that the ability of the sand to mobilize shear strength is also reduced with the increase in the amplitude of γ_Δ history.

Fig. 12 shows the relationship between the post-liquefaction peak undrained shear strength (τ_p) and γ_Δ. The τ_p is taken at the peak point on the stress-strain response for the loose and dense specimen from Fig. 7a and b, respectively. The data points are slightly scattered due to the difficulty in selecting the peak stress points on

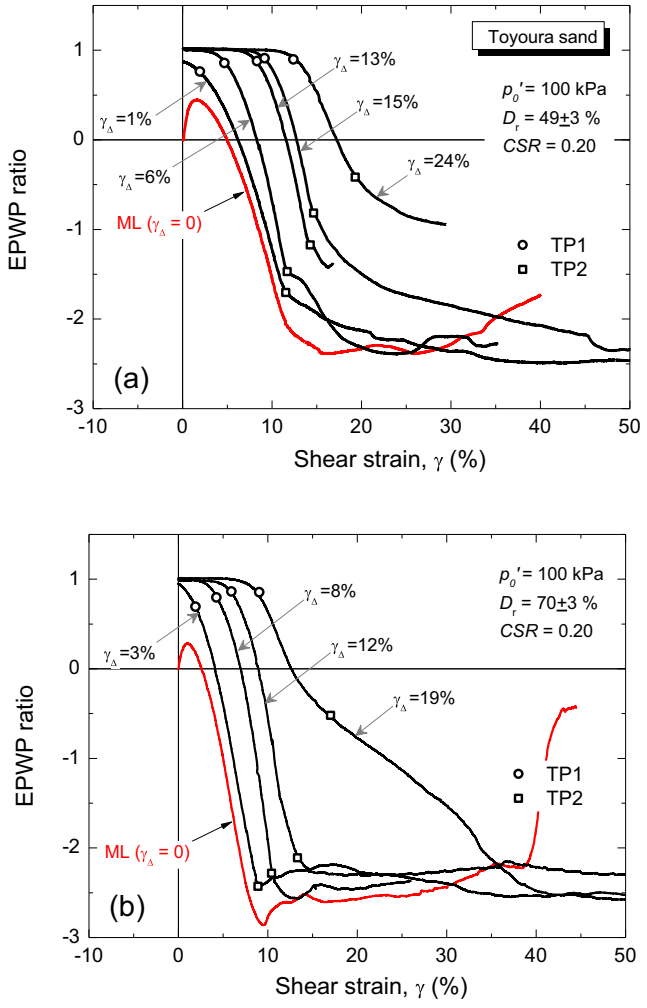

Fig. 8. Post-liquefaction excess pore water pressure (EPWP) ratios of (a) loose ($Dr = 49 \pm 3\%$) and (b) dense ($Dr = 70 \pm 3\%$) in undrained torsional shear tests with various damage strain levels.

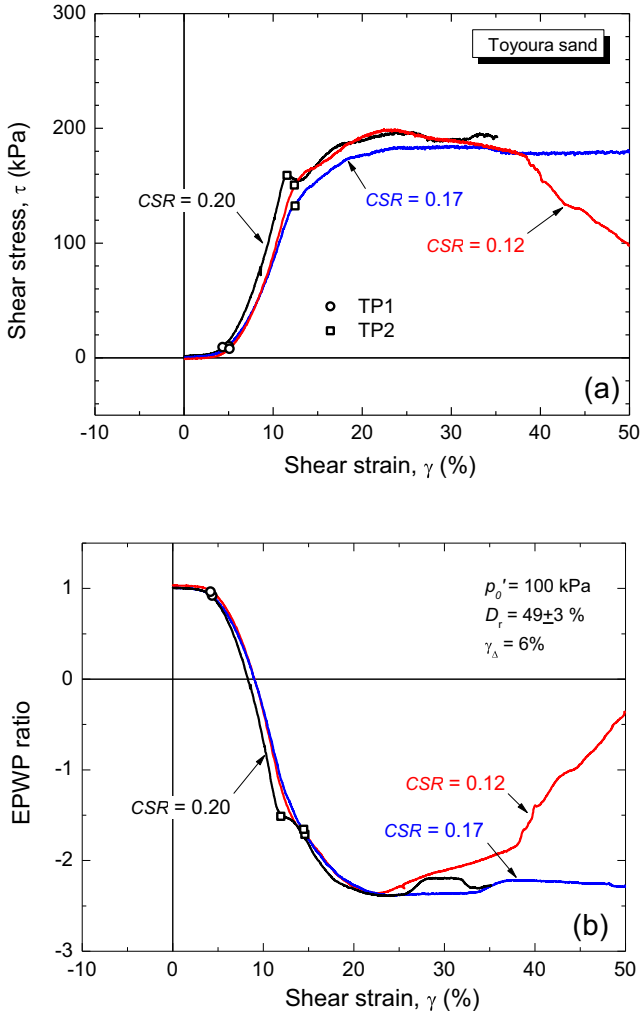

Fig. 9. Post-liquefaction undrained torsional shear response of loose sand ($Dr = 49 \pm 3$) for various level of cyclic stress ratio: (a) stress-strain relationships; and (b) EPWP trends.

the stress-strain plot after the TP2, e.g. $\gamma_\Delta = 3\%$ in Fig. 7b. That is, in some tests there is a smooth transition into a residual stress state with a drop of shear stress associated with strain softening. In other tests, however, the stress continued to increase irregularly after the TP2, e.g. $\gamma_\Delta = 6\%$ in Fig. 7a. Such characteristics are the consequence of strain localization in the specimens (Kiyota et al., 2008; Chiaro et al., 2013) during monotonic shearing as described in the subsequent section.

An attempt was made to utilize such valuable data points and estimate the following: (1) the maximum values of τ_p ($\tau_{p,max}$) expected under monotonic post-liquefaction undrained shear conditions if $\gamma_\Delta = 0$ (i.e. just after the full liquefaction state but with no γ_Δ developed), and (2) the minimum values of τ_p ($\tau_{p,min}$) expected under monotonic post-liquefaction undrained shear conditions when the maximum feasible value of γ_Δ (before strain localization during undrained cyclic shear loading takes place) is applied. To do so, the $\gamma_{\Delta,max}$ values were established based on the relationship between relative density and cyclic limiting strain shown in Fig. 12b (note that the proposed linear trend provides an upper bound of the limiting shear strain observed in undrained cyclic shear tests – i.e. liquefaction tests without damaging strain – and it coincides with the level of maximum shear strain measured in the field and in physical tests for liquefied sandy soils as reported by Kiyota et al., 2008, 2013. Consequently, the $\tau_{p,max}$ and $\tau_{p,min}$ for $D_r = 49 \pm 3\%$ are 204 kPa and 46 kPa, respectively. Besides, the $\tau_{p,max}$ and $\tau_{p,min}$ for $D_r = 70 \pm 3\%$ are 275 kPa and 176 kPa, respectively.

3.3. Influence of strain localization on post-liquefaction deformation and strength characteristics of sand

Fig. 13a shows the variation of differential stress ($\sigma_d = \sigma_v' - \sigma_h'$) with the shear strain (γ) in undrained ML(NL) tests without γ_Δ for four loose specimens ($D_r = 49 \pm 3\%$) consolidated at p_0' of 100, 150, 200 to 400 kPa. Since the tests were performed under the isotropic stress condition ($\sigma_v' = \sigma_h'$) and the vertical deformation of

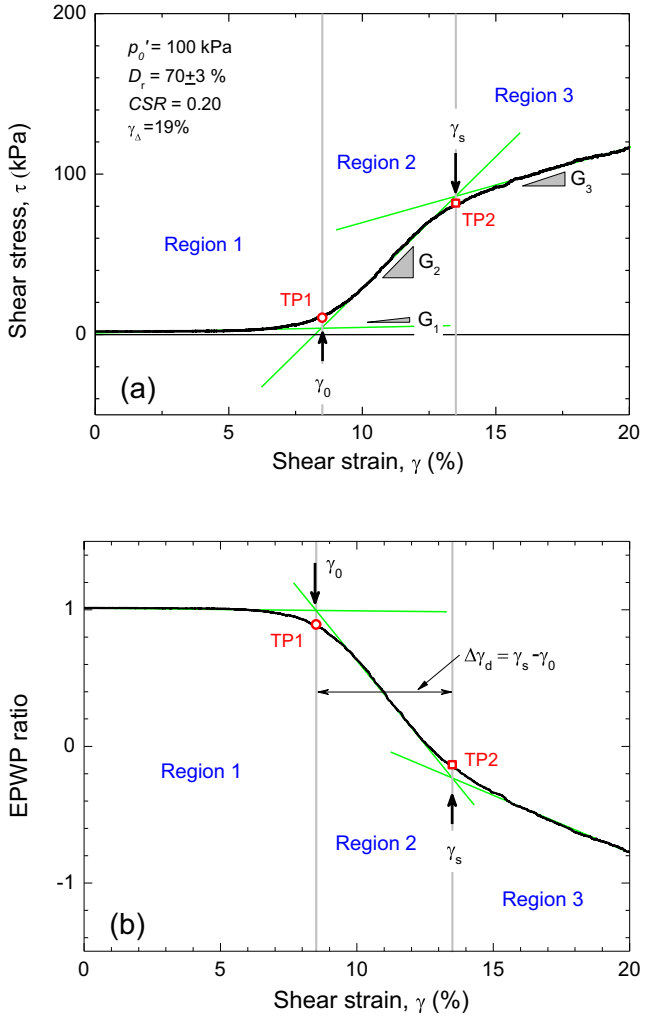

Fig. 10. Definition of proposed three-region post-liquefaction undrained behavior based on threshold (γ_0) and dilative ($\Delta\gamma_d$) strains.

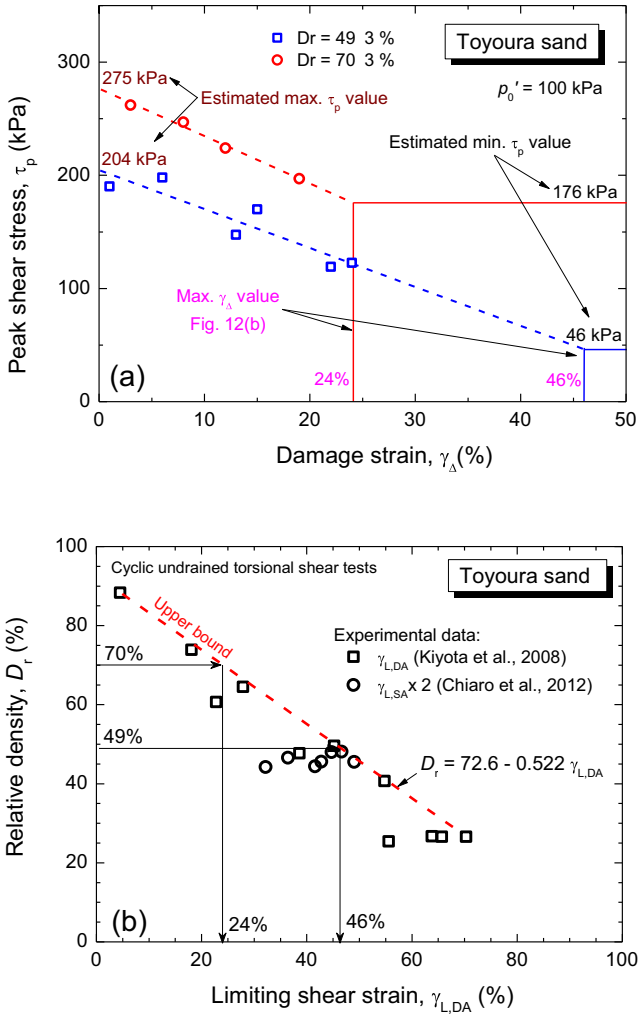

Fig. 12. (a) Relationships between post-liquefaction undrained peak shear strength and damage strain; and (b) Relationship between relative density and limiting shear strain in cyclic undrained torsional shear tests.

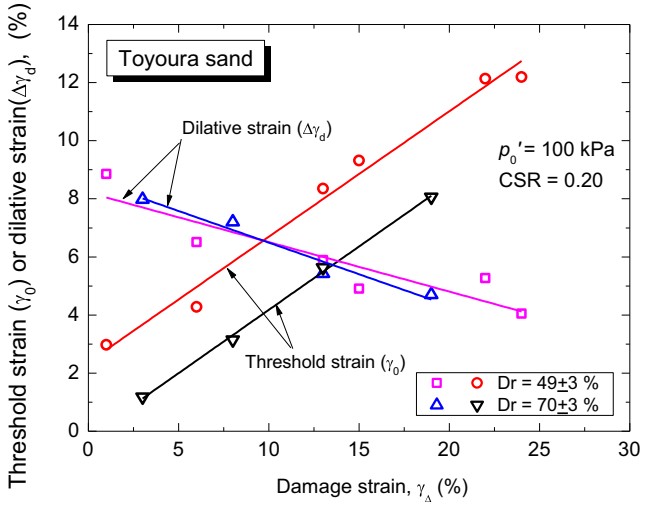

Fig. 11. Relationships between threshold strain vs. damage strain and dilative strain vs. damage strain.

the specimens was maintained to be zero, any increase or decrease in the σ_d describes the dilatancy characteristic of the specimens. The test results show that during the ML, the specimens' positive dilatancy is mobilized (positive value of σ_d) and subsequently achieved a peak stress state with the absolute peak value of σ_d.

Despite the difference in the confining stress, the specimens exhibited similar tendencies, while the value of the σ_d increased with the p_0' level. Such test results indicate that the increase in p_0' mobilizes a tendency towards greater positive dilatancy in specimens with the same density state. The results also show that a sudden drop of σ_d was observed at the same level of γ. The sudden drop of σ_d' indicates the initiation of non-uniform deformation in the specimen as reported by Kiyota et al. (2008) and Chiaro et al. (2013). Also, the shear strain amplitude at the drop of σ_d was referred to as the limiting shear strain (γ_L) to initiate strain localization. Kiyota et al. (2008) showed that γ_L is greater for loose specimens as compared to that of dense specimens in undrained cyclic loading (refer to Fig. 12b). In

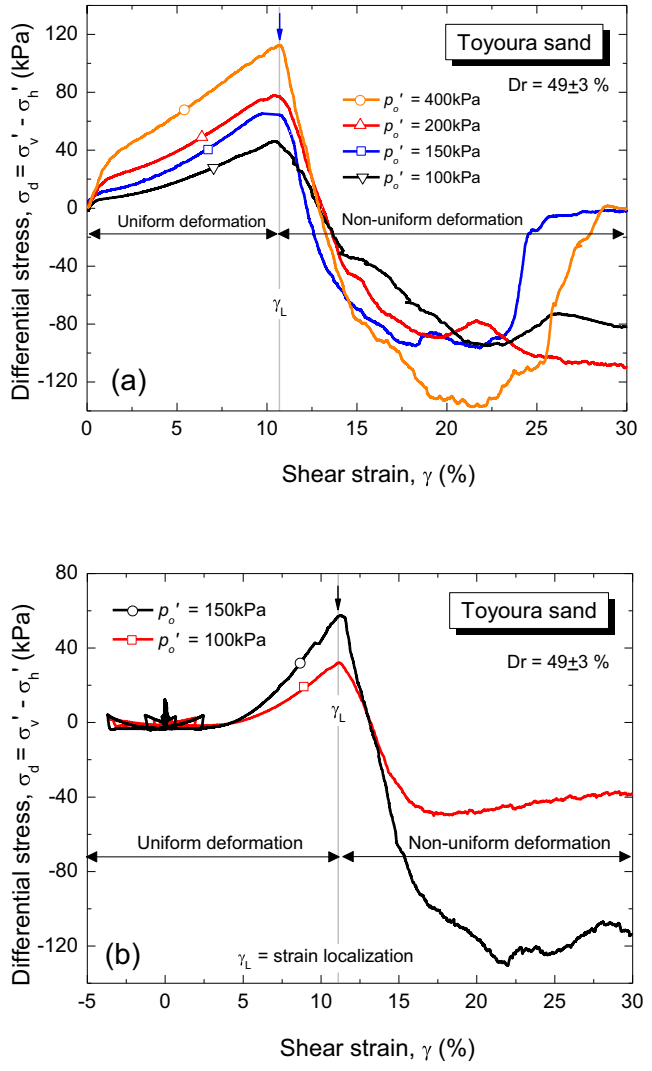

Fig. 13. Differential stress variation with shear strain for undrained monotonic loading: no damage strain; and (b) 6% damage strain.

the present study, it is found that γ_L is independent of the p_0' for specimens with identical density in the undrained ML(NL) tests.

The specimen deformation during undrained ML at several states as numbered 1 through 6 is shown in Photo 1 for the specimen with $p_0' = 100$ kPa (i.e., Test 1–1). The deformation of the specimen remained uniform throughout the height of the specimen up to a single amplitude shear strain (γ_{SA}) of 10%. The shear bands (A-A and B-B in Photo 1) appeared between $\gamma_{SA} = 10\%$ and 20%. At $\gamma_{SA} = 25\%$, three shear bands A-A, B-B, and C-C formed along the specimen height. The specimen's behavior after $\gamma_{SA} = 25\%$ was affected by deformation non-uniformity and various wrinkles appeared on the specimen's surface.

Fig. 13b shows the relationship of σ_d and γ for two multi-stage tests (cyclic test followed by the undrained ML) consolidated at $p_0' = 100$ kPa (i.e., Test 3–1) and 150 kPa (i.e., Test 3–2), respectively. In both tests $\gamma_\Delta = 6\%$ developed under $CSR = 0.20$. Despite the difference in the isotropic consolidation stress, a drop in the σ_d occurred at the same level of γ, suggesting that the specimens' γ_L to initiate strain localization is independent of the initial consolidation stress also in multi-stage tests with the same history of γ_Δ. The specimen deformation for the multistage Test 3–2 at several states as numbered 1 through 4 is shown in Photo 2. The photos show that the deformation in the specimen remained uniform throughout the height up to $\gamma_{SA} = 10\%$. The shear band (marked by the dotted circle in Photo 2) appeared at around $\gamma_{SA} = 12\%$, at state 3. At state 4, $\gamma_{SA} = 15\%$, the specimen displacement above the shear band is greater than that developed in the bottom part of the specimen. Comparison of deformation of the liquefied specimen (Photo 2) and non-liquefied specimen (Photo 1) suggests that the shear band(s) formation brought the specimen to failure.

Fig. 14a and b show the relationship of σ_d with γ in multi-stage tests on loose specimens subjected to a γ_Δ of

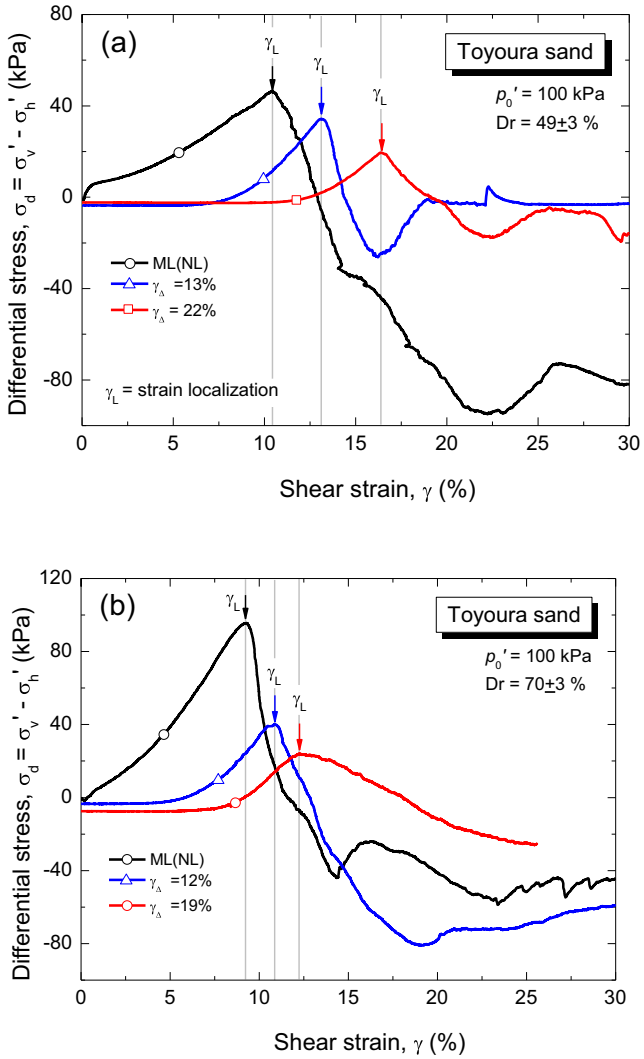

Fig. 14. Differential stress variation with shear strain for various damage strain for (a) loose and (b) dense Toyoura sand and its comparison with a ML test without undrained cyclic history.

13% and 22% and dense specimens with a γ_Δ of 12% and 19%, respectively. The specimens were consolidated at p_0' = 100 kPa. Two observations can be made from Fig. 14a and b. Firstly, an increase in the γ_Δ resulted in the reduction in the value of σ_d for both the loose and dense specimens. Such reduction is expected and associated with the softening effect induced by straining the specimen. Secondly, the value of γ_L increased with the increase in the γ_Δ. This indicates that the cyclic straining delays the strain localization in the specimen. A comparison between the tests suggests that the γ_L level is different for specimens with and without γ_Δ consolidated at the same p_0'.

To further describe the post-liquefaction behavior of sand specimens, a multi-stage test with $\gamma_\Delta = 22\%$ is plotted independently in Fig. 15. A butterfly shape can be seen in Fig. 15a in the cyclic loading stage, during which the σ_d repeatedly recovered. Close-up views of the ML sand response during the initial recovery part and the sudden drop of σ_d are plotted in Fig. 15b and c. It can be observed from Fig. 15b, that after TP1, there is an accelerated recovery in the σ_d. Moreover, in Fig. 15c, a sudden drop of σ_d is plotted in combination with the corresponding shear stress in the dotted line. The change in the slope of the stress-strain in Fig. 15c refers to the sudden drop of σ_d. This suggests that TP 2 on the stress-strain in the multi-stage tests resulted from the change in the specimen's behavior due to strain localization.

Fig. 16 shows the relationship between single amplitude limiting strain ($\gamma_{L,SA}$)and γ_Δ for the loose and dense Toyoura sand specimens consolidated at p_0' = 100 kPa. The plot suggests that there are two linear relationships between γ_L and γ_Δ, one for the loose specimens and the other for the dense specimens. Furthermore, it seems there exists a lower boundary for γ_L, which is related to the maximum amount of γ_Δ that can be applied for loose and dense Toyoura sand specimens in undrained cyclic torsional shear tests before strain localization occurs (refer to Fig. 12b).

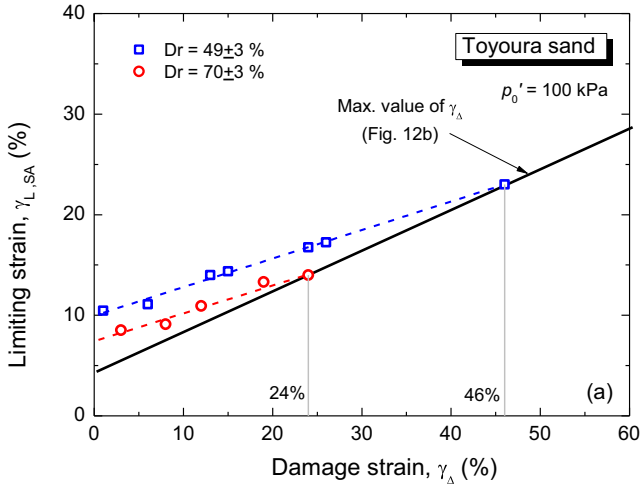

Fig. 16. Relationships between limiting strain and damage strain for loose and dense Toyoura sand.

The occurrence of strain localization increases the difficulty of accurately interpreting the experimental results, especially in the case of sandy soils bounded by a latex membrane preventing the smooth evolution of shear band(s). The concept of strain as an average quantity becomes inadequate and local shear and local pore water pressure are seldom measurable. At a large strain level,

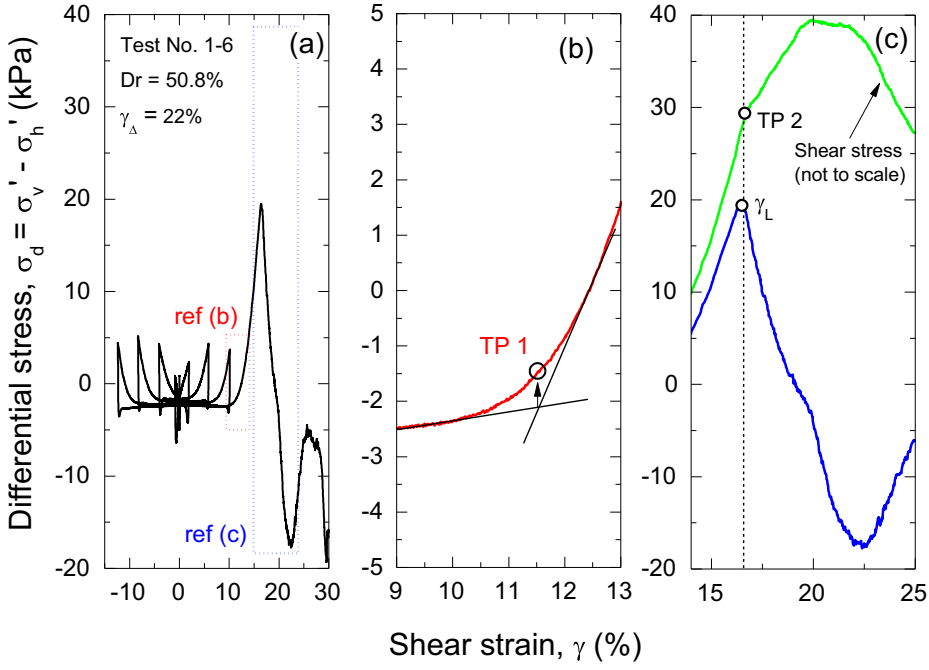

Fig. 15. Differential stress response for damage strain of 22%.

the global void ratio is an average value for the specimen and does not reflect the condition of the soil at a critical state. The critical state maybe is only reached in the shear band during undrained loading, and it can be argued that the soil fabric that develops is not "critical state fabric" (Oda and Kazama, 1998). Therefore, measured global parameters after initiation of the shear band(s) become a specimen size and boundary condition dependent rather than true load-deformation behavior of soil. The test results showed that the drop of the σ_d demarcates the region of uniform to non-uniform deformation in the specimen and was validated through 3D image analysis by Henry et al. (2019). Also, the results show that the softening strain (γ_s) occurred at the γ_L to initiate strain localization i.e. $\gamma_s = \gamma_L$. It can be concluded that during undrained torsional shearing, global stress-strain measurement by the external transducer is a true representative of the specimen characteristics until γ_L. After γ_L, the measurements will be highly affected by deformation non-uniformity in the specimen.

Therefore, in the present study, it is proposed that the undrained shear strength of sand should be taken until the state of uniform deformation in the specimen (i.e., a drop of the σ_d). The shear strength and EPWP at this state are defined as limiting peak undrained shear strength and limiting EPWP. The degree of degradation in a liquefied specimen is defined by the strength degradation ratio (τ_d) and EPWP degradation ratio (r_d) as defined by Eqns. (2) and (3):

- Strength degradation ratio,

$$\tau d = \frac{\tau PL^{\Delta}}{\tau PL} \tag{2}$$

- EPWP degradation ratio,

$$rd = \frac{\Delta Ucyc}{\Delta U} \tag{3}$$

where,

τ_{PL} = Undrained limiting strength in the reference ML (with $\gamma\Delta = 0$ after liquefaction)

$\tau_{PL\Delta}$ = Undrained limiting strength in ML with γ_Δ

ΔU = EPWP ratio in undrained ML without γ_Δ

ΔU_{cyc} = EPWP ratio in undrained ML with γ_Δ

For sands without degradation, τ_d and r_d are equal to 1, and τ_d<1 will indicate the degree of strength deterioration in reference with the ML test with $\gamma_\Delta = 0$.

Fig. 17a shows the relationship between τ_d and γ_Δ. For both densities, despite the difference in the effective mean stress and cyclic shear stress ratio, the data points follow similar trends, indicating that the undrained strength rapidly degrades with increasing γ_Δ. For instance, at the γ_Δ = 15%, a loose specimen possesses only 60% of the strength from the initial state.

For completeness, the data points shown in Fig. 17a are replotted in Fig. 17b in terms of τ_d vs. $\gamma_\Delta/\gamma_{L,DA}$ (where the latter is the uniformity coefficient – i.e. for $\gamma_\Delta/\gamma_{L,DA} < 1$, specimen deformation is uniform and unaffected by strain localization during undrained cyclic loading). It is

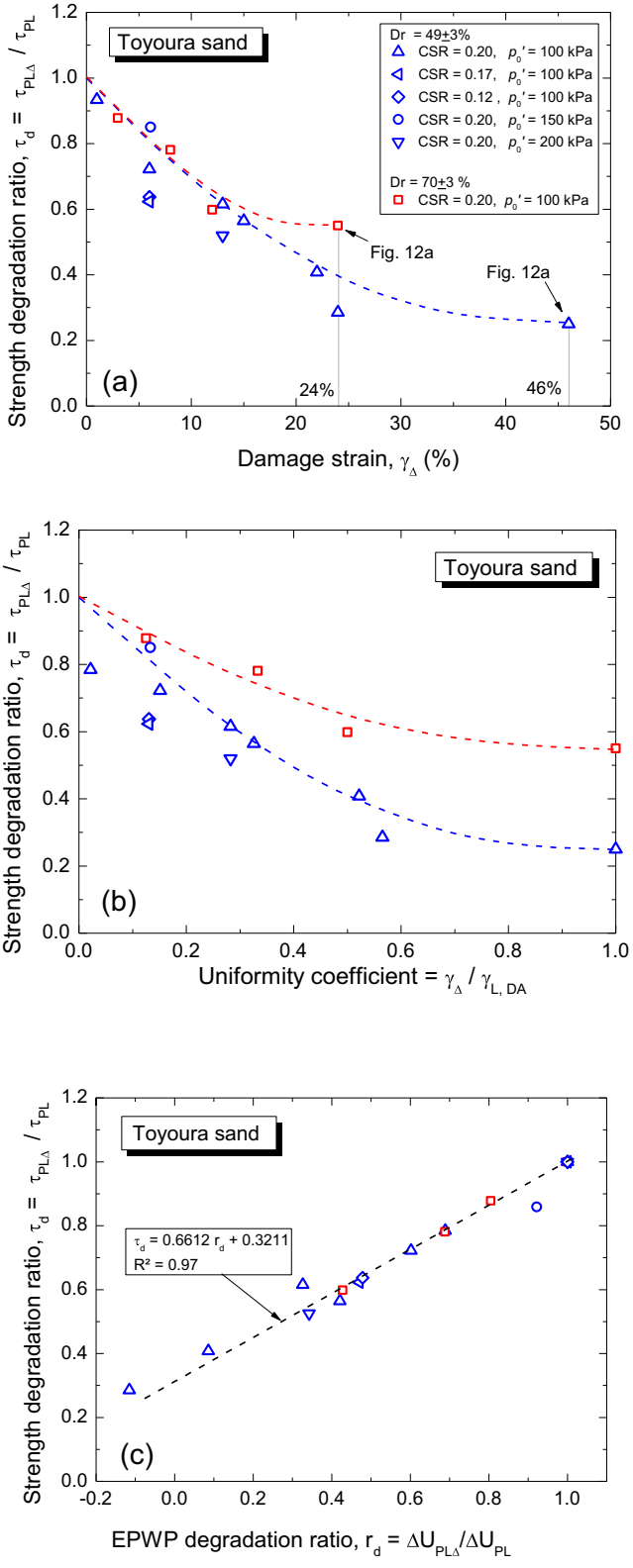

Fig. 17. Relationships between strength degradation strength ratio and: (a) damage strain; (b) uniformity coefficient; and (c) EPWP degradation ratio.

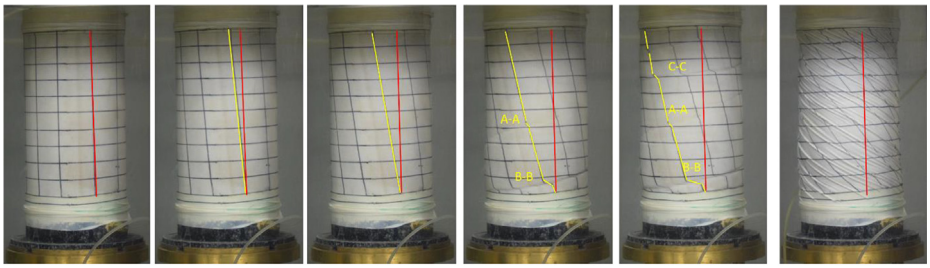

State1 $\gamma_{SA} = 0$ | State 2 $\gamma_{SA} = 5\%$ | State 3 $\gamma_{SA} = 10\%$ | State 4 $\gamma_{SA} = 20\%$ | State 5 $\gamma_{SA} = 25\%$ | State 6 $\gamma_{SA} = 30\%$

Photo 1. Specimen's deformation in ML test without damage strain (Test. No. 1-1).

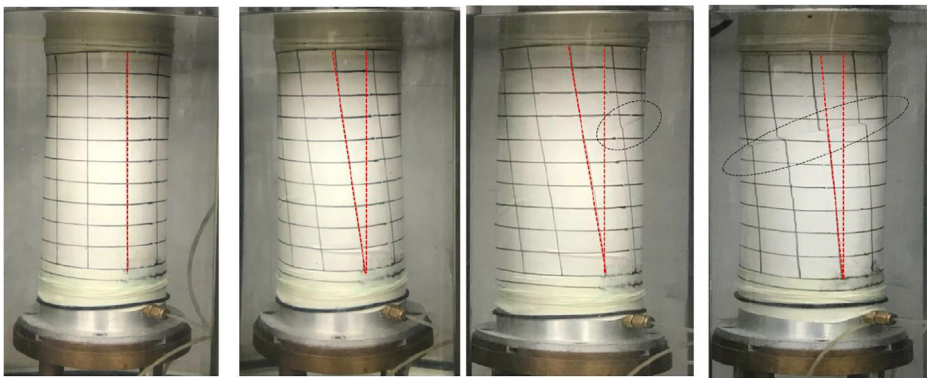

State1 $\gamma_{SA} = 0$ | State 2 $\gamma_{SA} = 7.5\%$ | State 3 $\gamma_{SA} = 12\%$ | State 4 $\gamma_{SA} = 15\%$

Photo 2. Specimen's deformation in a post-liquefaction ML test with damage strain of 6% (Test. No. 3-2).

confirmed, therefore, that for all the tested Toyoura specimens, the deformation was uniform during cyclic loading (before ML. It is worth mentioning that, if $\gamma_{\Delta}/\gamma_{L,DA} \geq 1$, then the deformation of the specimens are not uniform and, hence, are affected by strain localization during undrained cyclic loading (before ML). In other words, the results of such tests are not suitable for use in evaluating the post-liquefaction characteristics of sand.

Fig. 17c shows the relationship between τ_d and r_d and it can be seen that the degradation is unaffected by the initial density, mean effective stress and cyclic shear stress ratio. In this case, a linear correlation can be established among the data points. In a similar way, Yasuhara and Toyota (1997) reported a degradation for Keuper Marl silt under the non-reversal stress condition in triaxial tests. However, the tendency of silt degradation was much slower as than that of the Toyoura sand. This could be associated with the material dependency on the degradation tendency subjected to cyclic loading. It is also possible that stress reversal and non-reversal may have induced different types of degradation in soils.

4. Conclusions

In this study, to study the post-liquefaction undrained strength and deformation characteristics of sand, a series of multi-stage liquefaction tests were performed on loose and dense Toyoura sand specimens by using a large-strain hollow cylindrical torsional shear apparatus. Based on the test results the following conclusions can be made:

1) The post-liquefaction stress-strain response can be differentiated into three regions during undrained monotonic loading. The *Region 1* spans from the state at which the sand specimen develops shear strain under zero effective stress and nearly-zero shear modulus (G_1). The *Region 2* corresponds to the transition point after the threshold shear strain (γ_0). The specimen transitioned into an intermediate state shear modulus (G_2) with the accelerated recovery in strength at a constant shear modulus. *Region 3* commences with the change in the stress-strain curve slope and specimen transitioned into the residual state shear modulus (G_3).

2) It was observed that strain localization brought the specimens to failure in undrained ML tests. Based on the responses of the differential stress, the stress and strain behavior is divided into uniform and non-uniform deformation regions. The stress and strain at the beginning of the non-uniform deformation state are defined as limiting undrained shear stress and strain, respectively. Strain localization depends on the mode of loading. For instance, in monotonic undrained shear loading, the limiting strain was the smallest, while the limiting strain in the case of cyclic loading was the largest. Strain localization is found to be independent of the confining stress and cyclic stress ratio, but is dependent on the amplitude of the damage strain developed during initial cyclic loading.
3) The post-liquefaction undrained shear strength is significantly affected by the damage shear strain. Specifically, irrespective of the density state, the damage shear strain decreases with increases in the damage strain level. Two degradation correlations are proposed to consider the effect of relative density, effective mean stress and cyclic stress ratio. A correlation between strength degradation ratio and damage strain is established to estimate the degradation of limiting shear stress due to the development of damage strain with reference to the undrained monotonic loading test without damage strain. A second correlation is proposed to calculate the degradation tendency of limiting strength ratio and the excess pore water pressure ratio.

Acknowledgments

The first author would like to acknowledge the Asian Development Bank for providing a PhD scholarship to study in the Civil Engineering Department of the University of Tokyo. The authors acknowledge the technical assistance provided by Toshihiko Katagiri, Technical Director, Institute of Industrial Science.

References

Ampadu, S.I.K., 1991. Undrained behavior of kaolin in torsional simple shear. Ph.D. Thesis, Department of Civil Engineering. University of Tokyo, Japan.

Boulanger, R.W., Chan, C.K., Seed, R.B., Seed, H.B., Sousa, J.B., 1993. A low-compliance bi-directional cyclic simple shear apparatus. Geotech. Test. J. 16 (1), 36–45.

Chiaro, G., De Silva, L.I.N., Koseki, J., 2017. Modeling the effects of static shear on the undrained cyclic torsional simple shear behavior of liquefiable sand. Geotech. Eng. J. 48 (4), 1–9.

Chiaro, G., Kiyota, T., Koseki, J., 2013. Strain localization characteristics of loose saturated Toyoura sand in undrained cyclic torsional shear tests with initial static shear. Soils Found. 53 (1), 23–34.

Chiaro, G., Koseki, J., Sato, T., 2012. Effects of initial static shear on liquefaction and large deformation properties of loose saturated Toyoura sand in undrained cyclic torsional shear tests. Soils Found. 52 (3), 498–510.

Chiaro, G., Umar, M., Kiyota, T., Koseki, J., 2021. Deformation and cyclic strength characteristics of sand under sloping ground conditions: insights from cyclic undrained torsional shear tests with static shear. Geotech. Eng. J. 52 (1), 10.

Dash, S., 2010. Lateral pile–soil interaction in liquefiable soils. Oxford: PhD thesis, University of Oxford, Oxford, UK.

Duttine, A., Tatsuoka, F., Shinbo, T., Mohri, Y., 2018. A new simplified seismic stability analysis taking into account degradation of soil undrained stress-strain properties and effects of compaction. Validation of Dynamic Analyses of Dams and Their Equipment - Edited Contributions to the International Symposium on the Qualification of Dynamic Analyses of Dams and Their Equipments 2016, 215–234.

Georgiannou, V.N., Tsomokos, A., Stavrou, K., 2008. Monotonic and cyclic behaviour of sand under torsional loading. Geotechnique 58 (2), 113–124.

Henry, M., Umar, M. & Kiyota, T., 2019. Quantification of the field of shear strains in saturated sand subjected to undrained monotonic and cyclic torsional shearing via 3D digital image correlation. Roma, Italy, Proc. of the 7th International Conference on Earthquake Geotechnical Engineering.

Hyodo, M., Murata, H., Yasufuku, N., Fujii, T., 1991. Undrained cyclic shear strength and residual shear strain of saturated sand by cyclic triaxial tests. Soils Found. 31 (3), 60–76.

Hu, Q., Zhang, J.M., Wang, R., 2020. Quantification of Dilatancy during Undrained Cyclic Loading and Liquefaction. Comput. Geotech. 128 (2020) 103853.

Kiyota, T., Koseki, K., Sato, T., 2013. Relationship between limiting shear strain and reduction of shear moduli due to liquefaction in large strain torsional shear tests. Soil Dyn. Earthq. Eng. 49, 122–134.

Kiyota, T., Sato, T., Koseki, J., Abadimarand, M., 2008. Behavior of liquefied sands under extremely large strain levels in cyclic torsional shear tests. Soils Found. 48 (5), 727–739.

Koseki, J., Yoshida, T., Sato, T., 2005. Liquefaction properties of Toyoura sand in cyclic tortional shear tests under low confining stress. Soils Found. 45 (5), 103–113.

Lombardi, D., Dash, S.R., Bhattacharya, Ibraim, E., Muir Wood, D. Taylor, C.A., 2017. Construction of simplified design p–y curves for liquefied soils. Geotechnique, 67, 3, 216–227.

McManus, K.J., Davis, R.O., 1997. Dilation-induced pore fluid cavitation in sands. Géotechnique 47 (1), 173–177.

Oda, M., Kazama, H., 1998. Microstructure of shear bands and its relation to the mechanisms of dilatancy and failure of dense granular soils. Geotechnique 48 (4), 465–481.

Rouholamin, M., Bhattacharya, S., & Orense, R.P., 2017. Effect of initial relative density on the post-liquefaction behaviour of sand. Soil Dynam. Earthq. Eng., 97, December 2016, 25–36.

Seed, H.B., 1987. Design problems in soil liquefaction. J. Geotech. Eng. 113 (8), 827–845.

Shamoto, Y., Zhang, J., Goto, S., 1997. Mechanism of large post-liquefaction deformation in saturated sand. Soils Found. 37 (2), 71–80.

Song, B.W., Yasuhara, K., Murakami, S., 2004. Direct simple shear testing for post-cyclic degradation in stiffness of nonplastic silt. Geotech. Test. J. 27 (6), 607–613.

Tatsuoka, F., Koseki, J., Takahashi, A., 2017. Earthquake-induced damage to earth structures and proposal for revision of their design based on a case history of the 2011 Off the Pacific Coast of Tohoku Earthquak. Journal of JSCE 5 (1), 101–112.

Tatsuoka, F., Muramatsu, M., Sasaki, T., 1982. Cyclic undrained stress-strain behavior of dense sands by torsional simple shear stress. Soils Found. 22 (2), 55–70.

Umar, M., Chiaro, G., Kiyota, T., Ullah, N., 2021. Deformation and cyclic resistance of sand in large-strain undrained torsional shear tests with initial static shear stress. Soils Found. https://doi.org/10.1016/j.sandf.2021.02.008 (in press).

Umar, M., Kiyota, T., Chiaro, G., 2018. Effect of specimen size on behavior of dense sand in large strain torsional shear apparatus. Bull. Earthq. Resistant Struct. Res. Center 51, 1–10.

Vaid, Y.P., Thomas, J., 1995. Liquefaction and postliquefaction behavior of sand. J. Geotech. Eng. 121 (2), 163–173.

Wang, R., Fu, P., Zhang, J.M., Dafalias, Y.F., 2016. DEM study of fabric features governing undrained post-liquefaction shear deformation of sand. Acta Geotech. 11 (6), 1321–1337.

Yasuda, S., Nagase, H., Mine, K., Yoshida, N., Kiku, H., Masuda, T., 1995. Stress–strain relationships of liquefied sands. Proceedings of the 1st international conference on earthquake geotechnical engineering, pp. 811–816.

Yasuhara, K., Toyota, N., 1997. Effects of initial static shear stress on postcyclic degradation of a plastic silt. Proc., 14th Int. Conf. on Soil Mechanics and Foundation Engineering, pp. 439–442.

Zhang, J.M., Wang, G., 2012. Large post-liquefaction deformation of sand, part I: physical mechanism, constitutive description and numerical algorithm. Acta Geotech. 7 (2), 69–113.